Chemical Science

ROYAL SOCIETY OF CHEMISTRY

EDGE ARTICLE

View Article Online
View Journal | View Issue

Cite this: *Chem. Sci.*, 2023, **14**, 13191

All publication charges for this article have been paid for by the Royal Society of Chemistry

Electron transport through supercrystals of atomically precise gold nanoclusters: a thermal bi-stability effect†

Tatsuya Higaki, ‡[a] Jake C. Russell,‡[b] Daniel W. Paley,[c] Xavier Roy *[b] and Rongchao Jin *[a]

Received 30th May 2023
Accepted 25th October 2023

DOI: 10.1039/d3sc02753h

rsc.li/chemical-science

Nanoparticles (NPs) may behave like atoms or molecules in the self-assembly into artificial solids with stimuli-responsive properties. However, the functionality engineering of nanoparticle-assembled solids is still far behind the aesthetic approaches for molecules, with a major problem arising from the lack of atomic-precision in the NPs, which leads to incoherence in superlattices. Here we exploit coherent superlattices (or supercrystals) that are assembled from atomically precise $Au_{103}S_2(SR)_{41}$ NPs (core dia. = 1.6 nm, SR = thiolate) for controlling the charge transport properties with atomic-level structural insights. The resolved interparticle ligand packing in $Au_{103}S_2(SR)_{41}$-assembled solids reveals the mechanism behind the thermally-induced sharp transition in charge transport through the macroscopic crystal. Specifically, the response to temperature induces the conformational change to the R groups of surface ligands, as revealed by variable temperature X-ray crystallography with atomic resolution. Overall, this approach leads to an atomic-level correlation between the interparticle structure and a bi-stability functionality of self-assembled supercrystals, and the strategy may enable control over such materials with other novel functionalities.

Introduction

Stimuli-responsive materials of molecules or organometallics can show dramatically improved functionalities owing to the tailoring strategy by molecular chemistry.[1] In contrast, the functionality engineering of self-assembled colloidal nanoparticles (NPs)[2] still lags behind the aesthetic approaches for molecules, although research on the NP systems has made tremendous progress in controlling the packing structures[2–4] as well as surface functionalization for versatile nanomaterials.[5–7] The major problem hindering the realization of molecular-precision assembly of NPs arises from the lack of atomic-precision of those NPs in both the core and the surface shell of ligands. While much work on charge transport in nanoparticle assemblies has been reported, the inherent size dispersity of conventional NPs (*e.g.* standard deviation of ~5%) and their elusive surface structure preclude the attainment of atomically coherent superlattices (*i.e.* supercrystals), because the coherence from the crystalline cores of NPs to the nanometer periodicity of superlattices is destroyed by the rotation of NPs and random packing of interparticle ligands in the NP assemblies.[8] Therefore, no atomic-level insight could be achieved.[8,9]

It has long been a major dream to obtain atomically precise NPs and assemble them into atomically coherent superlattices for achieving versatile functionalities.[5,6,10] Recent advances in nanochemistry[11–17] have offered access to gold NPs with atomically precise cores and definitive numbers of surface ligands (*e.g.*, thiolate –SR or phosphine PPh_3),[10,16,17] which are represented by exact formulae (*e.g.*, $Au_n(SR)_m$ for thiolate-protected NPs), akin to molecules.[18–21] Such ultrasmall NPs (1–3 nm core diameter) are often called nanoclusters (NCs). More importantly, crystallization of such NCs can lead to long-range coherence from the angstrom level to the macroscopic length scale (*e.g.*, millimeter) in the assemblies,[22–24] which offers new opportunities in transport measurements, including photoconductivity[25] and electrical conductivity.[26–29] The structural order is very important in charge transport.[27] Yuan *et al.*[28] discovered an anisotropic effect (in plane *vs.* out of plane) in supercrystals assembled from nanoclusters. In recent work, Zhu *et al.*[29] demonstrated an electronic spin-polarized transport (*i.e.* a spin valve effect) in assembled nanoclusters by observing a magnetoresistance of 1.6% even at room temperature, which was attributed to the spin–orbit coupling (SOC) effect of NCs.

[a]*Department of Chemistry, Carnegie Mellon University, Pittsburgh, Pennsylvania 15213, USA. E-mail: rongchao@andrew.cmu.edu*

[b]*Department of Chemistry, Columbia University, New York, New York 10027, USA. E-mail: xr2114@columbia.edu*

[c]*Columbia Nano Initiative, Columbia University, New York, New York 10027, USA*

† Electronic supplementary information (ESI) available. See DOI: https://doi.org/10.1039/d3sc02753h

‡ These authors contributed equally.

Here we report a thermally-induced sharp transition (*i.e.* a bistability effect) in electron transport through supercrystals self-assembled from atomically-precise gold NCs, including $Au_{103}S_2(SR)_{41}$, $Au_{133}(SR)_{52}$, and $Au_{144}(SR)_{60}$. As for $Au_{103}S_2(SR)_{41}$, the interparticle ligand packing structure is rationalized to be responsible for the thermally responsive transition of charge transport through the atomically coherent crystals. X-ray crystallography with atomic resolution (0.8–1.1 Å) reveals that the response to external temperature induces conformational changes to the naphthalene groups of surface ligands. The obtained structural insights reveal a correlation between the surface structure and functionality of self-assembled supercrystals with atomically-precise gold NPs. The strategy described here will help material scientists to improve the tailoring method for atomic-level control over nanostructures and solid materials for novel functionalities.

Results and discussion

The atomically precise $Au_{103}S_2(SR)_{41}$, $Au_{133}(SR)_{52}$, and $Au_{144}(SR)_{60}$, where the R groups are 2-naphthalene, 4-*tert*-butyl benzene, and benzyl group, respectively, were synthesized by "size-focusing" and/or "ligand-exchange" methods,[30–32] followed by supercrystal growth. The as-prepared crystals were then used for current–voltage (*I–V*) measurements at variable temperatures (from 300 K down to 120 K) to study thermal-responsive conductivity of the NC self-assembled crystal. The stimuli-responsive conductivity is further correlated with the structural changes by performing X-ray crystallography at different temperatures.

Charge transport through the Au_{103} supercrystal

We first discuss the charge transport properties of the $Au_{103}S_2(SR)_{41}$-assembled crystals (Au_{103} for short). The synthesis of atomically-precise Au_{103} was performed by a ligand-exchange reaction from $Au_{99}(SPh)_{42}$ with 2-naphthalenethiol.[30] A vapor diffusion of methanol into 1,2,4-trichlorobenzene solution of Au_{103} yielded needle-shaped crystals. Each Au_{103} NC shows an atomically-precise structure made up of a Au_{79} core protected by oligomeric $-S-(Au^I-S)_n-$ motifs which can be called "staples" (Fig. 1a), and the crystal exhibits a rod-like morphology (Fig. 1b and c). The crystal is in a monoclinic crystal system with *C*2/*c* space group. Crystallographic face indexing determined the longitudinal axis of the crystals as [001], thus, the charge

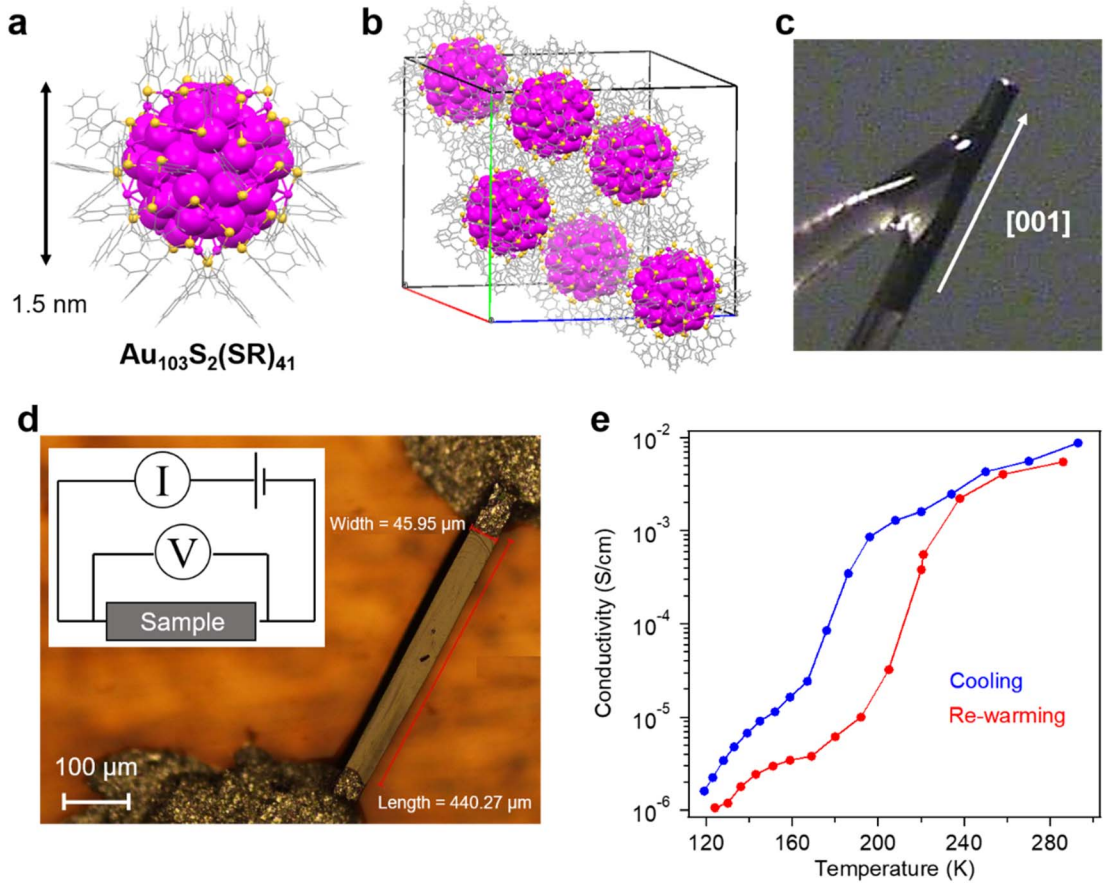

Fig. 1 Self-assembled crystal of atomically-precise Au_{103} NCs for charge transport measurement. (a) Crystal structure of $Au_{103}S_2(SR)_{41}$. (b) Unit cell of a single crystal of Au_{103}. (c) Face indexing of a Au_{103} crystal to determine the long axis. (d) Charge transport study on a Au_{103} assembled crystal along the [001] direction. (e) Conductivity of a Au_{103} assembled crystal at variable temperatures.

transport measurements were performed along the [001] axis of single crystals (Fig. 1b and c). Both ends of the crystal were covered by silver paste in order to form good contacts (Fig. 1d). At room temperature, the conductivity (σ) of a typical Au_{103} crystal was $\sim 10^{-2}$ S cm^{-1}. Interestingly, it drastically decreased to $\sim 10^{-6}$ S cm^{-1} at 120 K with a sharp drop (~two orders of magnitude) over 196–167 K (Fig. 1e).

Upon re-warming, the conductivity gradually increases with increasing temperature to 192 K, followed by a sharp increase of conductivity over 192 to 238 K. The hysteresis loop shows a two-orders-of-magnitude difference at ~180 K (mid-point) for cooling and at ~210 K for re-warming (Fig. 1e). Such a hysteresis is reversible, indicating no thermally caused damage to particle arrangements in the crystal or other irreversible processes.

The conductance in the Au_{103}-assembled crystal increased with temperature, indicating that thermal activation (k_BT) is required to overcome the energy barriers between NCs.[33,34] This is typical of the charge hopping mechanism,[35,36] and the activation energy is expressed by the equation:

$$\sigma(d, T) = \sigma_0 e^{-\beta d} e^{-E_A/k_B T} \quad (1)$$

where, d is the interparticle distance (Å), T is the temperature (K), β is the electron-tunneling coefficient, and E_A is the activation energy (eV). A system with weak electronic coupling is known for this type of conducting behavior (such as the highly disordered organics or NPs' film).[37–40] Therefore, our observation indicates that the charge carriers are localized in each NP, resulting in smaller interparticle electronic coupling ($\beta << k_BT$). The plot from eqn (1) shows that the activation barriers in the Au_{103} crystal varied in different temperature ranges (see Fig. S1†), with the activation energies determined to be I: 0.12 eV (293–196 K), II: 0.35 eV (196–167 K), and III: 0.093 eV (167–119 K). These values are comparable to E_A values in weakly coupled organic crystals.[41]

Sizes and energy-gaps of nanoclusters

To investigate the potential NC size and bandgap (E_g) effects, we compared the charge transport properties of Au_{103} crystals with other crystals assembled from $Au_{133}(SR')_{52}$ or $Au_{144}(SR'')_{60}$ (Fig. S2 and S3†). All these are thiolate-protected (with >100 Au atoms) and show clearly resolved carbon tail structures by X-ray crystallography (Fig. S2 and S3†). Under the same measurement conditions, the crystals exhibited a trend of decreasing conductivity with cooling, and the room temperature conductivity is similar ($\sim 10^{-2}$ S cm^{-1}) among the crystals of 3 sizes of NCs, indicating negligible effects of energy-gaps of each type of NCs (note: the E_g varies from 0.5 eV of Au_{103} to 0.1 eV of Au_{144}); thus, the core sizes are less critical, rather the ligands should play a more important role. Among the three systems, the naphthalenethiolate-protected Au_{103} crystals showed the most distinctive thermal responsivity (width of the hysteresis: ~40 K, Fig. 1e), while the $Au_{144}(SR'')_{60}$ crystal (where R'' = benzyl group) showed a similar two-orders of magnitude transition but a much less prominent hysteresis due to less extensive C–H$\cdots\pi$ interaction of the smaller benzene ring (Fig. S3b†) than the naphthalene groups on Au_{103} (Fig. S4†), and the case of $Au_{133}(SR')_{52}$ (R' = 4-*tert*-butyl benzene) exhibited neither transition nor hysteresis due to the almost destroyed C–H$\cdots\pi$ interaction by the *tert*-butyl group on the benzene ring (Fig. S2b†). Overall, the observed trend implies the important role of the ligand type and the interparticle ligand packing in the crystal.

Variable temperature single crystal XRD analysis

In order to obtain further structural insight into the thermally-induced sharp transition and hysteresis in the Au_{103} crystal, variable temperature single crystal XRD (SCXRD) was performed (Fig. 2). We find that Au_{103} NCs are linearly assembled along the [001] direction of the crystal, which is the same direction as the charge transport (Fig. 2a). The metal core structures do not show any change during the cooling/rewarming processes. Fig. 2b summarizes temperature-dependent unit cell lengths normalized by cell volume. Upon re-warming from 120 K, the crystal experiences an elongation along the [001] direction, which continues with the temperature rise to 240 K. Above 240 K, the unit cell starts to shrink along the [001] direction until reaching room temperature. The unit cell length along the *b*-axis shows opposite changes: a gradual decrease between 120 K and 240 K but an increase between 240 and 300 K. The schematic illustration of NC arrangement is shown in Fig. 2c. It is interesting to observe that the unit cell parameters for *b*- and *c*-axis show volcano-like behavior with the transition temperature at ~240 K upon re-warming (Fig. 2b). This temperature is indeed comparable to the temperature of sharp conductivity changes during the re-warming process. Thus, the correlation between the observed temperature-induced changes for unit cell parameters and conductivity suggests that the sharp conductivity transition should be induced by the interparticle conformational change in response to external heat. Previous work on charge transport in NP assemblies[42,43] could not observe any sharp transition possibly because of the polydispersity of NPs and lack of atomic-level coherence. In our system, we observed a two-orders-of-magnitude variation in conductivity over the sharp transition and distinct hysteresis behavior in the atomically coherent assembly of precise NPs. The underlying mechanism is revealed by resolving interparticle ligands' conformation.

The conformation-induced transition/hysteresis mechanism is also supported by the much less distinct behavior in the cases of Au_{133} or Au_{144} crystals that do not show a linearly-assembled wire-like structure with interlocked aromatic carbon tails of naphthalene groups; note that the potential interlocking of *tert*-butylbenzene groups in the Au_{133} sample is destroyed by *tert*-butyl, whereas the benzyl groups in the Au_{144} sample can partially interlock but much less than the naphthalene case. Therefore, the distinct transition/hysteresis in Au_{103} crystals should originate from the linearly assembled Au_{103} NCs along the [001] direction, which is the direction of the measured electrical conductance, and the conformational changes to interparticle naphthalene groups along the [001] induces the sharp transition due to the phase transition between the less conductive conformation (yet more stable) at low-T and the

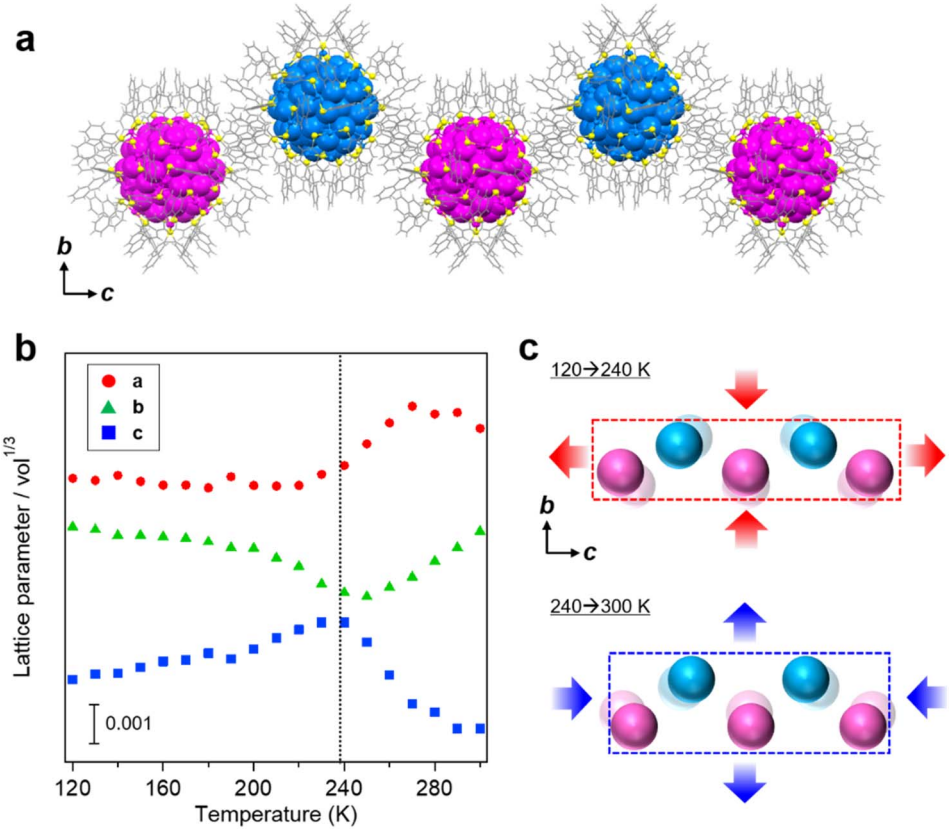

Fig. 2 Variable temperature SCXRD analysis of a Au_{103}-assembled crystal. (a) Packing of Au_{103} NCs along [001] direction (the *c* axis) in the crystal. Blue and magenta illustrate Au atoms in different Au_{103} enantiomers. (b) Unit cell parameters at 120–300 K normalized by cell volume. (c) Schematic illustration of rearrangement of Au_{103} NCs while re-warming.

more conductive conformation at high-T. While molecular packing is involved in the charge transport properties of organic crystals,[44–46] the systems of thiolate-protected NCs are much more complex due to the inorganic/organic hybrid and spherical topology (as opposed to planar organic molecules, which involves relatively simple π–π stacking interactions). In randomly assembled films of atomically precise NCs[25,26] or coherent crystals without interlocked aromatic groups,[27,28] no coherent effect of ligands was observed. In order to resolve the changes with atomic resolution, we further performed full-structural analysis by X-ray crystallography at 210 and 300 K, respectively, and the obtained insights are discussed below.

First of all, ample C–H···π interactions are found in the crystal of Au_{103} NCs. The intra-particle C–H···π distance is 2.58 ± 0.08 Å, which is considerably shorter than 2.73 ± 0.13 Å for typical C–H···π distance in organic crystals.[47] In addition, the Au_{103} NCs are linearly assembled *via* C–H···π interaction between the surface-protecting 2-naphthalenethiolate ligands (Fig. 3a). Of note, the interparticle distance (core center-to-center) is 23.74 Å along the *c*-axis (Fig. S4†), while for other directions the nearest distances (27.41 Å and 27.48 Å) are significantly longer. Thus, the charge hopping should largely proceed along the *c*-axis or [001] direction. Charge carriers are considered to travel through the interlocked naphthalene groups as highlighted in Fig. 3a during the charge transport along the [001] axis. At 300 K, the interparticle ligands' C–H···π interactions show a distance of 2.920 Å, which increases to 2.941 Å at 210 K, hence, the conductivity drops at low temperatures. Further insights into the conformational changes are obtained for adjacent ligands (noted as L_1 and $L_{1'}$) near interlocked ligands (Fig. 3b). Interestingly, at 210 K, conformational disorders are observed for these neighboring ligands, which are not observed at 300 K. This observation suggests that the decrease in conductivity is induced by the conformational changes of interparticle ligands' interactions, rather than the interparticle distance (invariant at 210 K and 300 K). Although the observed structure difference does not seem large, more dramatic changes are expected to be observed at much lower temperatures considering the significantly lower conductivity (see above Fig. 1e).

We note that the non-linear assembly in the cases of Au_{133} and Au_{144} crystals and their lack of strong inter-locking pattern of ligands lead to significantly less distinct transition and hysteresis in the crystals of Au_{133} and Au_{144} compared to the naphthalenethiolate-protected Au_{103} NCs.

Thermal analysis on the transition

We further carried out differential scanning calorimetry (DSC) analysis between −150 and 50 °C (123–323 K, Fig. 4). Two reversible transformations were observed in the crystal

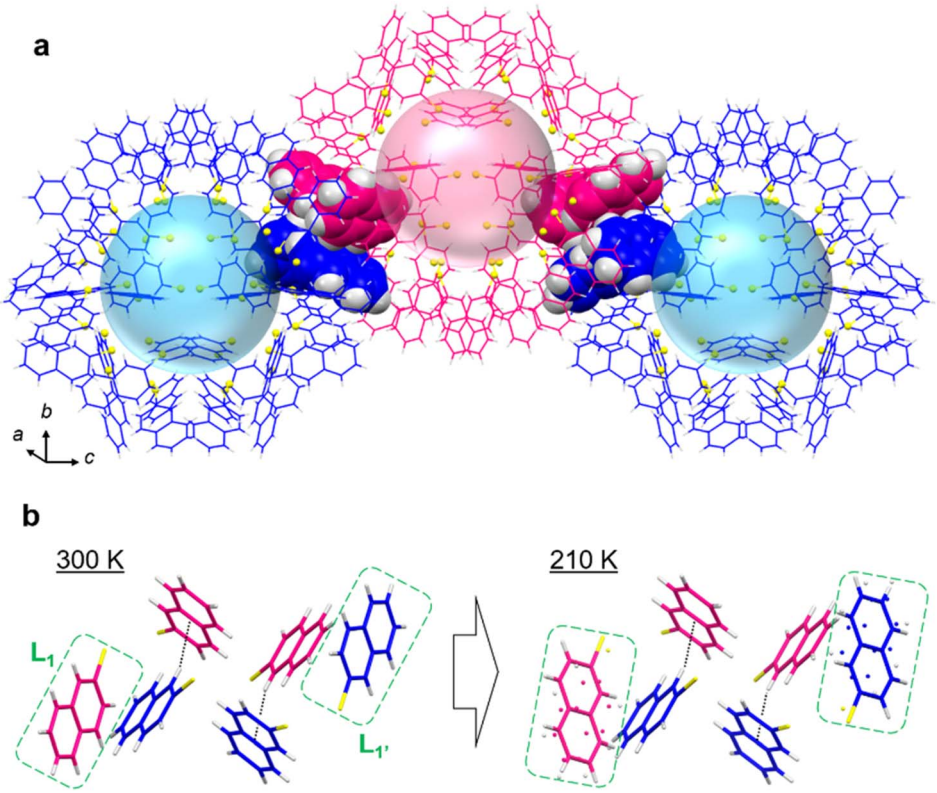

Fig. 3 Carbon tail structures between self-assembled Au_{103} NCs. (a) Packing of Au_{103} along the [001] direction with highlights in interlocked naphthalene carbon tails between adjacent NCs. (b) Temperature-dependent conformation changes in interparticle C–H···π interactions for interlocked naphthalene carbon tails.

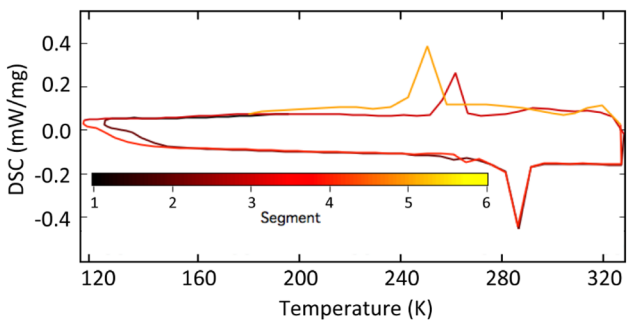

Fig. 4 DSC analysis of the phase transition in the supercrystal assembled from Au_{103} NCs.

assembled from Au_{103} NCs, and the transition observed in DSC occurs near the temperature of the transition in the conductivity measurements, indicating that the electron transport change was induced by the phase transition, consistent with the X-ray crystallographic analysis.

Conclusions

In summary, this work presents the discovery of thermally induced sharp transition and hysteresis of conductivity in crystals assembled from atomically precise Au_{103} NCs and reveals atomic-level insight into the structural correlation with charge transport properties. The crystals exhibit charge hopping transport with decrease in conductivity upon cooling, due to the weak interparticle electronic coupling, and abrupt changes in activation energy are revealed by Arrhenius-like plots. Further crystallographic analysis rules out the interparticle distance change and unravels the conformational changes to the interparticle ligands, the latter explains the temperature dependent conductivity as well as the thermal hysteresis. This work elucidates the critical role of interparticle ligands' conformation on the charge transport of assembled NPs with atomic-level coherence. The bi-stability behavior of coherent crystal materials of nanoclusters *via* ligand tailoring may hold potential in future exploration for memory, sensing, and actuation applications.

Data availability

All the data are included in the ESI; Crystallographic structure files (cif deposition numbers: 2 153 700 for Au_{103}–300 K, 2 153 701 for Au_{103}–210 K) can be retrieved at CCDC, **https://www.ccdc.cam.ac.uk**.

Author contributions

T. H. and J. C. R. contributed equally to this work. R. J. and X. R. conceived the project. T. H. performed all the synthesis and

single crystal growth. J. C. R. conducted the variable temperature charge transport measurements. D. W. P. collected and analyzed X-ray diffraction data at different temperatures. T. H., J. C. R., X. R. and R. J. wrote the manuscript with the contributions from all the other authors.

Conflicts of interest

There are no conflicts to declare.

Acknowledgements

We thank Dr Chong Liu, Dr Tian-Yi Luo, and Prof. Nathaniel L. Rosi for face-indexing analysis of Au_{103} single crystal. R. J. acknowledges the financial support from the AFOSR (work of the synthesis of NCs). X. R. acknowledges the AFOSR funding for the electrical transport measurements under AFOSR Award no. FA9550-18-1-0020. J. C. R. is supported by the Department of Defense through the National Defense Science and Engineering Graduate (NDSEG) Fellowship.

References

1 O. Sato, Dynamic Molecular Crystals with Switchable Physical Properties, *Nat. Chem.*, 2016, **8**, 644–656.
2 M. A. Boles, M. Engel and D. V. Talapin, Self-Assembly of Colloidal Nanocrystals: From Intricate Structures to Functional Materials, *Chem. Rev.*, 2016, **116**, 11220–11289.
3 Q.-Y. Lin, J. A. Mason, Z. Li, W. Zhou, M. N. O'Brien, K. A. Brown, M. R. Jones, S. Button, B. Lee, V. P. Dravid, K. Aydin and C. A. Mirkin, Building Superlattices from Individual Nanoparticles *via* Template-Confined DNA-Mediated Assembly, *Science*, 2018, **359**, 669–672.
4 X. Huang, J. Zhu, B. Ge, K. Deng, X. Wu, T. Xiao, T. Jiang, Z. Quan, Y. C. Cao and Z. Wang, Understanding Fe_3O_4 Nanocube Assembly with Reconstruction of a Consistent Superlattice Phase Diagram, *J. Am. Chem. Soc.*, 2019, **141**, 3198–3206.
5 C. R. Kagan, E. Lifshitz, E. H. Sargent and D. V. Talapin, Building Devices from Colloidal Quantum Dots, *Science*, 2016, **353**, aac5523.
6 M. Zhang, D. J. Magagnosc, I. Liberal, Y. Yu, H. Yun, H. Yang, Y. Wu, J. Guo, W. Chen, Y. J. Shin, A. Stein, J. M. Kikkawa, N. Engheta, D. S. Gianola, C. B. Murray and C. R. Kagan, High-Strength Magnetically Switchable Plasmonic Nanorods Assembled from a Binary Nanocrystal Mixture, *Nat. Nanotechnol.*, 2017, **12**, 228–232.
7 R. Klajn, J. F. Stoddart and B. A. Grzybowski, Nanoparticles Functionalised with Reversible Molecular and Supramolecular Switches, *Chem. Soc. Rev.*, 2010, **39**, 2203–2237.
8 Y. Nagaoka, R. Tan, R. Li, H. Zhu, D. Eggert, Y. A. Wu, Y. Liu, Z. Wang and O. Chen, Superstructures Generated from Truncated Tetrahedral Quantum Dots, *Nature*, 2018, **561**, 378–382.
9 L. Wu, J. J. Willis, I. S. McKay, B. T. Diroll, J. Qin, M. Cargnello and C. J. Tassone, High-Temperature Crystallization of Nanocrystals into Three-Dimensional Superlattices, *Nature*, 2018, **548**, 197–201.
10 M. Zhou, T. Higaki, G. Hu, M. Y. Sfeir, Y. Chen, D. Jiang and R. Jin, Three-Orders-of-Magnitude Variation of Carrier Lifetimes with Crystal Phase of Gold Nanoclusters, *Science*, 2019, **364**, 279–282.
11 W.-Q. Shi, Z.-J. Guan, J.-J. Li, X.-S. Han and Q.-M. Wang, Site-Specific Doping of Silver Atoms into a Au_{25} Nanocluster as Directed by Ligand Binding Preferences, *Chem. Sci.*, 2022, **13**, 5148–5154.
12 Y. Lin, Y. Cao, Q. Yao and J. Xie, Revealing the Composition-Dependent Structural Evolution Fundamentals of Bimetallic Nanoparticles through an Inter-Particle Alloying Reaction, *Chem. Sci.*, 2022, **13**, 4598–4607.
13 S. Hasegawa, S. Masuda, S. Takano, K. Harano, J. Kikkawa and T. Tsukuda, Synergistically Activated Pd Atom in Polymer-Stabilized $Au_{23}Pd_1$ Cluster, *ACS Nano*, 2022, **16**, 16932–16940.
14 X. Wei, C. Xu, H. Li, X. Kang and M. Zhu, Fabrication of a Family of Atomically Precise Silver Nanoclusters *via* Dual-Level Kinetic Control, *Chem. Sci.*, 2022, **13**, 5531–5538.
15 X.-M. Luo, S. Huang, P. Luo, K. Ma, Z.-Y. Wang, X.-Y. Dong and S.-Q. Zang, Snapshots of Key Intermediates Unveiling the Growth from Silver Ions to Ag_{70} Nanoclusters, *Chem. Sci.*, 2022, **13**, 11110–11118.
16 S. Kenzler and A. Schnepf, Metalloid Gold Clusters - Past, Current and Future Aspects, *Chem. Sci.*, 2021, **12**, 3116–3129.
17 A. J. Touchton, G. Wu and T. W. Hayton, $[Ni_{30}S_{16}(PEt_3)_{11}]$: an Open-Shell Nickel Sulfide Nanocluster with a "Metal-Like" Core, *Chem. Sci.*, 2022, **13**, 5171–5175.
18 Y. Zhu, J. Guo, X. Qiu, S. Zhao and Z. Tang, Optical Activity of Chiral Metal Nanoclusters, *Acc. Mater. Res.*, 2020, **2**, 21–35.
19 C. Zeng, Y. Chen, K. Kirschbaum, K. J. Lambright and R. Jin, Emergence of Hierarchical Structural Complexities in Nanoparticles and Their Assembly, *Science*, 2016, **354**, 1580–1584.
20 N. Xia, J. Xing, D. Peng, S. Ji, J. Zha, N. Yan, Y. Su, X. Jiang, Z. Zeng, J. Zhao and Z. Wu, Assembly-Induced Spin Transfer and Distance-Dependent Spin Coupling in Atomically Precise AgCu Nanoclusters, *Nat. Commun.*, 2022, **13**, 5934.
21 W. Zhang, J. Kong, Y. Li, Z. Kuang, H. Wang and M. Zhou, Coherent Vibrational Dynamics of $Au_{144}(SR)_{60}$ Nanoclusters, *Chem. Sci.*, 2022, **13**, 8124–8130.
22 J. V. Rival, P. Mymoona, K. M. Lakshmi, Nonappa, T. Pradeep and E. S. Shibu, Self-Assembly of Precision Noble Metal Nanoclusters: Hierarchical Structural Complexity, Colloidal Superstructures, and Applications, *Small*, 2021, **17**, 2005718.
23 S. Hossain, Y. Imai, Y. Motohashi, Z. Chen, D. Suzuki, T. Suzuki, Y. Kataoka, M. Hirata, T. Ono, W. Kurashige, T. Kawawaki, T. Yamamoto and Y. Negishi, Understanding and Designing One-Dimensional Assemblies of Ligand-Protected Metal Nanoclusters, *Mater. Horiz.*, 2020, **7**, 796–803.
24 Y. Li, M. Zhou, Y. Song, T. Higaki, H. Wang and R. Jin, Double-Helical Assembly of Heterodimeric Nanoclusters into Supercrystals, *Nature*, 2021, **594**, 380–384.

25 M. Galchenko, A. Black, L. Heymann and C. Klinke, Field Effect and Photoconduction in Au_{25} Nanoclusters Films, *Adv. Mater.*, 2019, **31**, 1900684.

26 M. Reato, T. Dainese, S. Antonello and F. Maran, Electron Transfer in Films of Atomically Precise Gold Nanoclusters, *Chem. Mater.*, 2021, **33**, 4177–4187.

27 (*a*) F. Fetzer, A. Maier, M. Hodas, O. Geladari, K. Braun, A. J. Meixner, F. Schreiber, A. Schnepf and M. Scheele, Structural Order Enhances Charge Carrier Transport in Self-Assembled Au-Nanoclusters, *Nat. Commun.*, 2020, **11**, 6188; (*b*) J. Hagel, M. T. Kelemen, G. Fischer, B. Pilawa, J. Wosnitza, E. Dormann, H. v. Löhneysen, A. Schnepf, H. Schnöckel, U. Neisel and J. Beck, Superconductivity of a Crystalline Ga84-Cluster Compound, *J. Low Temp. Phys.*, 2002, **129**, 133–142; (*c*) D. Bono, A. Schnepf, J. Hartig, H. Schnöckel, G. J. Nieuwenhuys, A. Amato and L. J. de Jongh, Muon Spin Relaxation Studies of Superconductivity in a Crystalline Array of Weakly Coupled Metal Nanoparticles, *Phys. Rev. Lett.*, 2006, **97**, 077601; (*d*) O. N. Bakharev, D. Bono, H. B. Brom, A. Schnepf, H. Schnöckel and L. J. de Jongh, Superconductivity in a Molecular Metal Cluster Compound, *Phys. Rev. Lett.*, 2006, **96**, 117002.

28 P. Yuan, R. Zhang, E. Selenius, P. Ruan, Y. Yao, Y. Zhou, S. Malola, H. Häkkinen, B. K. Teo, Y. Cao and N. Zheng, Solvent-Mediated Assembly of Atom-Precise Gold–Silver Nanoclusters to Semiconducting One-Dimensional Materials, *Nat. Commun.*, 2020, **11**, 2229.

29 Y. Zhu, L. Guo, J. Guo, L. Zhao, C. Li, X. Qiu, Y. Qin, X. Gu, X. Sun and Z. Tang, Room-Temperature Spin Transport in Metal Nanocluster-Based Spin Valves, *Angew. Chem., Int. Ed.*, 2023, **62**, e202213208.

30 T. Higaki, C. Liu, T.-Y. Luo, N. R. Rosi and R. Jin, Tailoring the Structure of 58-Electron Gold Nanoclusters: $Au_{103}S_2(S\text{-}Nap)_{41}$ and Its Implications, *J. Am. Chem. Soc.*, 2017, **139**, 9994–10001.

31 C. Zeng, Y. Chen, K. Kirschbaum, K. Appavoo, M. Y. Sfeir and R. Jin, Structural Patterns at All Scales in a Nonmetallic Chiral $Au_{133}(SR)_{52}$ Nanoparticle, *Sci. Adv.*, 2015, **1**, e1500045.

32 N. Yan, N. Xia, L. Liao, M. Zhu, F. Jin, R. Jin and Z. Wu, Unraveling the Long-Pursued Au_{144} Structure by X-Ray Crystallography, *Sci. Adv.*, 2018, **4**, eaat7259.

33 J. M. Wessels, H.-G. Nothofer, W. E. Ford, F. von Wrochem, F. Scholz, T. Vossmeyer, A. Schroedter, H. Weller and A. Yasuda, Optical and Electrical Properties of Three-Dimensional Interlinked Gold Nanoparticle Assemblies, *J. Am. Chem. Soc.*, 2004, **126**, 3349–3356.

34 Y. Wang, C. Duan, L. Peng and J. Liao, Dimensionality-Dependent Charge Transport in Close-Packed Nanoparticle Arrays: from 2D to 3D, *Sci. Rep.*, 2014, **4**, 7565.

35 J. L. Brédas, D. Beljonne, V. Coropceanu and J. Cornil, Charge-Transfer and Energy-Transfer Processes in π-Conjugated Oligomers and Polymers: a Molecular Picture, *Chem. Rev.*, 2004, **104**, 4971–5003.

36 H. Oberhofer, K. Reuter and J. Blumberger, Charge Transport in Molecular Materials: an Assessment of Computational Methods, *Chem. Rev.*, 2017, **117**, 10319–10357.

37 W. P. Wuelfing and R. W. Murray, Electron Hopping through Films of Arenethiolate Monolayer-Protected Gold Clusters, *J. Phys. Chem. B*, 2002, **106**, 3139–3145.

38 A. Zabet-Khosousi and A.-A. Dhirani, Charge Transport in Nanoparticle Assemblies, *Chem. Rev.*, 2008, **108**, 4072–4124.

39 Q. Li, J. C. Russell, T.-Y. Luo, X. Roy, N. L. Rosi, Y. Zhu and R. Jin, Modulating the Hierarchical Fibrous Assembly of Au Nanoparticles with Atomic Precision, *Nat. Commun.*, 2018, **9**, 3871.

40 W. P. Wuelfing, S. J. Green, J. J. Pietron, D. E. Cliffel and R. W. Murray, Electronic Conductivity of Solid-State, Mixed-Valent, Monolayer-Protected Au Clusters, *J. Am. Chem. Soc.*, 2000, **122**, 11465–11472.

41 A. Ueda, S. Yamada, T. Isono, H. Kamo, A. Nakao, R. Kumai, H. Nakao, Y. Murakami, K. Yamamoto, Y. Nishio and H. Mori, Hydrogen-Bond-Dynamics-Based Switching of Conductivity and Magnetism: a Phase Transition Caused by Deuterium and Electron Transfer in a Hydrogen-Bonded Purely Organic Conductor Crystal, *J. Am. Chem. Soc.*, 2014, **136**, 12184–12192.

42 A. Zabet-Khosousi and A.-A. Dhirani, Charge Transport in Nanoparticle Assemblies, *Chem. Rev.*, 2008, **108**, 4072–4124.

43 J.-Y. Kim and N. A. Kotov, Charge Transport Dilemma of Solution-Processed Nanomaterials, *Chem. Mater.*, 2014, **26**, 134–152.

44 J. C. Sancho-García, A. J. Pérez-Jiménez, Y. Olivier and J. Cornil, Molecular Packing and Charge Transport Parameters in Crystalline Organic Semiconductors from First-Principles Calculations, *Phys. Chem. Chem. Phys.*, 2010, **12**, 9381–9388.

45 A. Datta, S. Mohakud and S. K. Pati, Comparing the Electron and Hole Mobilities in the α and β Phases of Perylene: Role of π-stacking, *J. Mater. Chem.*, 2007, **17**, 1933–1938.

46 O. Ostroverkhova, Organic Optoelectronic Materials: Mechanisms and Applications, *Chem. Rev.*, 2016, **116**, 13279–13412.

47 M. Nishio, The CH/π Hydrogen Bond in Chemistry. Conformation, Supramolecules, Optical Resolution and Interactions Involving Carbohydrates, *Phys. Chem. Chem. Phys.*, 2011, **13**, 13873–13900.